

Link Performance Improvement via Design Variables Optimization in LED-Based VLC System for Inter-satellite Communication

David N. Amanor
ECE Department

North Carolina A&T State University
Greensboro, NC 27401
Email: dnamanor@aggies.ncat.edu

William W. Edmonson
ECE Department

North Carolina A&T State University
Greensboro, NC 27401
Email: wwedmons@ncat.edu

Fatemeh Afghah

School of Informatics, Comp. & Cyber Sys.
Northern Arizona University
Flagstaff, Arizona 86001
Email: fatemeh.afghah@nau.edu

Abstract—In our previous paper, we examined the utility of LEDs for inter-satellite communication (ISC) in multiple small satellite networks and proposed an approach of the physical layer design that meets the requirements of the platform in terms of the critical physical layer design variables. These variables (or parameters) include the LED transmit power, photodetector active area, receiver bandwidth and link distance. One of the most important tasks for the visible light communication (VLC) system designer is how to ensure the required balance or trade-off among these variables in order to achieve the desired performance. In this work, we employed multi-objective optimization to determine physical layer design variables at which the signal-to-noise ratio (SNR) at the VLC receiver is maximized. We used the Non-dominated Sorting Genetic Algorithm II (NSGA-II) in MATLAB to determine the Pareto front of two conflicting objective functions, and then extracted the optimal solution using the Technique for Order of Preference by Similarity to Ideal Solution (TOPSIS). Analysis of the optimal solution showed that it yielded the maximum SNR within the set of non-dominated solutions at the Pareto front. We showed that using multi-objective optimization techniques for assignment of parameter values can yield more than 3 dB improvement in the SNR.

I. INTRODUCTION

Recent advancement in LED technology has triggered renewed interest in visible light communication (VLC) as a viable alternative to RF and LASER for establishing inter-satellite communication links in multiple small satellite networks. This has become increasingly important due to the diminishing volume of RF spectrum bandwidth below the 6 GHz band for high data rate communication [1]. The inter-satellite communication links (ISLs) in these multi-satellite networks are also much shorter than links between satellites in geostationary orbit; thus, the use of LASER and the highly accurate pointing they provide can be considered superfluous [2]. With approximately 300 THz of free bandwidth available for VLC, high capacity data transmission rates could be provided over short distances using LEDs and photodetectors.

The problem with small satellites is that they are constrained by the size limitations for housing onboard power sources and communication subsystem electronics. The basic single unit, 1U standard CubeSat, must occupy a volume not exceeding 10 cm x 10 cm x 10 cm units, with a mass not exceeding 1.33 kg per unit [3]. Although a 1U CubeSat can be expanded to higher configuration if more capability is required, it is crucial to resist the creep toward larger and more expensive CubeSat

missions, as this defeats the primary goal of maintaining low-cost approaches as the cornerstone of CubeSat development [4].

These limitations bring to the fore the need to ensure optimal allocation of resources, in terms of the balance or trade-off of key design parameters required, to achieve the desired performance. One way to address these constraints in the physical layer is to use components that have small footprints, are light weight, and have low power requirements. For short to medium range ISLs, we proposed a high-level description of an LED-based VLC system as seen in [5] for ISC. Our motivation for using LEDs is due to their small size, light weight and low power requirements, as well as their long lifetime and low cost. A further advantage is the abundant bandwidth available in the visible band which could be exploited for high data-rates ISC.

In [5], we developed an analytical model of the ISL and then investigated the performance of the link by varying key design parameters such as transmitted optical power P_t , photodetector active area A_{pd} , and receiver bandwidth B for a given link distance d . With this approach, which is similar to the approach used in earlier related works in [2] and [6], the analytical models were simulated using assumed parameter values for all design variables. However, this approach is not optimal especially in situations where design objectives are conflicting. For example, in a VLC link, the received signal power P_r and total noise variance N , are both directly dependent on the active photodetector area A_{pd} [5]. Any attempt to maximize the received power by increasing A_{pd} may result in making the noise worse. In such situations, using one's judgement alone to make a decision on the assignment of key parameter values to evaluate or simulate system performance may be suboptimal. One approach for achieving the required balance and ensure optimal assignment of design parameter values for a given design space is to employ multi-objective optimization techniques. Optimization techniques enable the communication system designer to answer a question such as: *What combination of transmitted optical power P_t , active photodetector area A_{pd} , and receiver bandwidth B , for a given link distance d , will yield the best SNR at the receiver?* In

other words, it replaces the inaccuracy of trial-and-error with a systematic and powerful tool that pinpoints the best solution.

Multi-objective optimization provides many optimal solutions, known as non-dominated solutions or Pareto-optimal front, except when the objectives are not conflicting in which case only one unique solution exists [7], [8]. A Pareto-optimal solution is better in at least one objective and concurrently worse in at least one other objective, when compared to another Pareto-optimal solution. Thus, the Pareto-optimal front provides decision makers deeper insight into the quantitative trade-off among objectives and then select one of the optimal solutions based on the results generated and their own judgment [7].

In this work, we employed the Non-dominated Sorting Genetic Algorithm II (NSGA-II) to determine the Pareto front of key design parameters required to achieve the desired SNR at the receiver, and then selected the optimal solution (i.e., solution with maximum SNR) from the Pareto front using the Technique for Order of Preference by Similarity to Ideal Solution (TOPSIS). Our preliminary evaluation of ten (10) different selection methods studied in [7] singles out TOPSIS as one out of two methods that consistently extracted an optimal solution that yielded the maximum SNR.

This paper is organized as follows; Sections 2 and 3 examined the VLC link and noise models, respectively. A formulation of the SNR of a VLC link for optimization is presented in Section 4. Section 5 discussed the NSGA-II and TOPSIS methods, and applied the methods to determine the optimal parameters for a given design space. Section 6 discussed performance improvement with and without optimization. The conclusion is captured in Section 7.

II. VLC LINK MODEL FOR ISC BETWEEN SMALL SATELLITES

Visible light communication systems use light rather than RF for wireless communication, and are classified as intensity modulated, direct detection (IM/DD) systems. The fundamental concept of an IM/DD channel, in relation to modulation and detection of optical intensities only, places a constraint on the type of signals which may be transmitted [9], [10]. The intensity modulated information bearing signal which is transmitted must remain non-negative for all time since the transmitted power can physically never be negative.

The line-of-sight (LOS) link between any two adjacent satellites in a trailing (or leader-follower) formation or within a cluster can be modelled according to the generic LOS VLC configuration illustrated in Fig. 1. The physical distance between the VLC transmitter and receiver is denoted by d , while the detector aperture radius and physical area are represented by r and A_{pd} , respectively. The symbols ψ and φ , represent the angle of incidence with respect to the receiver axis and angle of irradiance with respect to the transmitter perpendicular axis, respectively. The parameter φ is an indicator of how focused the beam is when emitted from the LED.

As shown in [12], the channel gain in LOS optical links can be estimated fairly accurately by considering only the LOS propagation path and can be expressed as

$$H(0) = \begin{cases} \frac{(m+1)}{2\pi d^2} A_{pd} (\cos\varphi)^m T_s g(\psi) \cos(\psi), & : 0 \leq \psi \leq \psi_c \\ 0, & : \psi > \psi_c \end{cases} \quad (1)$$

The filter transmission coefficient (or gain) and concentrator gain are represented by the parameters T_s and $g(\psi)$, respectively. The concentrator FOV semi-angle is denoted by ψ_c and m is the order of Lambertian emission (i.e., a number which describes the shape of the radiation characteristics).

As shown in [11] and [12], the Lambertian order m is related to the semi-angle at half illuminance of an LED, $\phi_{\frac{1}{2}}$ and is given by

$$m = \frac{-\ln 2}{\ln(\cos(\phi_{\frac{1}{2}}))} \quad (2)$$

By using a hemispherical lens (i.e., non-imaging concentrator) with internal refractive index n , we can achieve a gain of [13]

$$g(\psi) = \begin{cases} \frac{n^2}{\sin^2\psi_c} & : 0 \leq \psi \leq \psi_c \\ 0, & : \psi > \psi_c \end{cases} \quad (3)$$

A hemisphere can achieve $\psi_c \approx \frac{\pi}{2}$ and $g(\psi) \approx n^2$ over its entire FOV provided the hemisphere is sufficiently large in relation to the detector, i.e., $R > n^2 r$, where r and R represents the detector and hemisphere radii, respectively [12].

For a given receiver FOV, the effective signal-collection area $A_{eff}(\psi)$ of the detector is given by $A_{eff}(\psi) = A_{pd} \cos\psi$ where $|\psi| < FOV$.

In line-of-sight (LOS) optical links, the relationship between the received optical power P_r and the transmitted optical power P_t can be represented by [6], [5]

$$P_r = H(0) P_t \quad (4)$$

The quantity $H(0)$ represents the channel DC gain and it is the single most important quantity for characterizing LOS optical links.

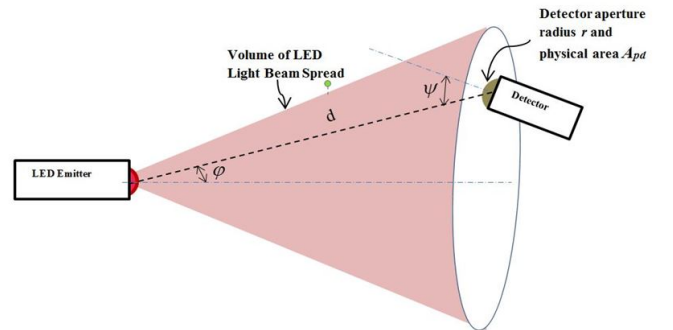


Fig. 1: LOS VLC Link Model: Adapted from [11]

It is important to note that (1) does not hold for non-Lambertian emission sources. For such sources, where the LEDs have particular beam shaping components, knowledge of the reshaped beam spatial distribution function $g_s(\theta)$ is needed in order to calculate the path loss [11].

Following from (4), the average received optical power P_r can be expressed as the sum of the transmitted power and path-loss on a dB scale, i.e., $P_r = P_t + H(0)$, where the channel has an optical path loss of $-10\log_{10}H(0)$ [measured in Optical decibels].

The electrical signal component S at the receiver side is given by [14]

$$S = (\gamma P_r)^2 \quad (5)$$

where γ represents the responsivity of the photodetector (in A/W).

Based on (1) and (4), the following assumptions hold fairly accurately for LOS optical links:

- 1) Path loss is assumed independent of wavelength,
- 2) Received optical power is inversely proportional to the square of the distance between the transmitter and receiver,
- 3) The photodetector detects light whose angle of incidence is less than the FOV, which is the acceptance angle of the detector.

III. THE NOISE MODEL

In this work, we considered the Sun as the main source of background illumination from the environment, and modelled it as a blackbody using Planck's blackbody radiation model, in which *spectral irradiance* of the source is a function of *wavelength* and *temperature* [14], i.e.,

$$W(\lambda, T) = \frac{2\pi h_p c^2}{\lambda^5} \frac{1}{(e^{\frac{h_p c}{\lambda k T}} - 1)} \quad (6)$$

where λ is the wavelength, c is the speed of light, h_p is Planck's constant, k is Boltzmann's constant and T is average temperature of the Sun's surface.

Following the approach of Spencer [15], we developed a simple yet fairly accurate analytical model that describes the irradiance that falls within the spectral range of the receiver optical filter

$$E_{det} \approx 2.15039x10^{-5} d_f t_f \int_{\lambda_a}^{\lambda_b} W(\lambda, T) d\lambda \quad (7)$$

where d_f and t_f are coefficients that represents the *day of the year* and *time of day*, respectively. For this work, we assume the maximum value for t_f , which is 1.0.

We validated our model by evaluating (7) for different wavelength intervals and compared the results with Solar Fluxes (W/m^2) taken from the 1985 Wehrli Standard Extraterrestrial Solar Irradiance Spectrum [16],[17].

The background noise power detected by the optical receiver physical area can be computed as [13]:

$$P_{bg} = E_{det} T_s A_{pd} n^2 \quad (8)$$

where T_s is the filter transmission coefficient and n is the internal refractive index of the concentrator at the receiver's optical front-end.

The total input noise variance N is the sum of the variances of the shot noise and thermal noise [13]:

$$N = \sigma_{shot}^2 + \sigma_{thermal}^2 \quad (9)$$

We neglect the effects of intersymbol interference (ISI) based on the assumption that the inter-satellite link between any two adjacent satellites in a leader-follower or cluster formation is not susceptible to multipath propagation.

The shot noise variance is given by [14]

$$\sigma_{shot}^2 = 2q\gamma(P_r + I_2 P_{bg})B \quad (10)$$

where q is the electronic charge, B is the equivalent noise bandwidth, γ represents the photodetector responsivity, and I_2 is the noise bandwidth factor for a rectangular transmitter pulse.

Following the analysis in [13], the thermal noise variance can be expressed by:

$$\sigma_{thermal}^2 = \frac{8\pi k T_A}{G} \eta A_{pd} I_2 B^2 + \frac{16\pi^2 k T_A \Gamma}{g_m} \eta^2 A_{pd}^2 I_3 B^3 \quad (11)$$

where k is Boltzmann's constant, T_A is the absolute temperature, G is the open-loop voltage gain, η is the fixed capacitance of photodetector per unit area, Γ is the FET channel noise factor, g_m is the FET transconductance and I_3 is the noise bandwidth factor for a full raised-cosine pulse shape [13].

Finally, the electrical SNR at the receiver, which is a key metric for measuring the quality of the communication link, can be determined by [5], [14], [18] and [19]

$$SNR = \frac{S}{N} = \frac{(\gamma P_r)^2}{\sigma_{shot}^2 + \sigma_{thermal}^2} \quad (12)$$

IV. FORMULATION OF SNR FOR OPTIMIZATION

For effective communication, the information or message signal should be dominant than the noise in the received signal in order to facilitate detection and decoding of the transmitted information signal. When noise increases beyond a certain threshold, the message would be distorted, which could lead to errors during detection and decoding. Thus, for reliable communication, it is important for the SNR per bit to be as large as possible in order to enhance signal detection and recovery at the receiver.

In this section, we applied multi-objective optimization to determine the optimal values of three key design parameters for achieving the maximum SNR at the VLC receiver. We formulated the SNR at the receiver in terms of two objective functions subject to three conflicting constraints of the system, namely, *LED transmit power* P_t , *photodetector area* A_{pd} , and *receiver bandwidth* B .

Following from (1), (4) and (9) - (12), the SNR can be expressed as

TABLE I: Simulation Model Parameter Assumptions

Parameter	Value
Semi-angle at Half Power, $\Phi_{\frac{1}{2}}$	30°
LED Peak Wavelength, λ_{peak}	656.2808 nm
Concentrator FoV Semi-angle, ψ_c	Varied: 35°
Filter Transmission Coefficient, T_o	1.0
Incidence Angle, φ	30°
Irradiance Angle, ψ	15°
Detector Responsivity, γ	0.51
Refractive Index of Lens, n	1.5
Radius of Concentrator, R	1.3 cm
Optical Filter Bandwidth, $\Delta\lambda$	0.4020 nm
Optical Filter Lower Limit, λ_1	656.0798 nm
Optical Filter Upper Limit, λ_2	656.4818 nm
Open Loop Voltage Gain, G	10
FET Transconductance, g_m	30 ms
FET Channel Noise Factor, Γ	0.82
Capacitance of Photodetector, η	38 pF/cm^2
Link Distance, d	1 km
Background Noise Power, P_{bg}	1 mW
Noise Bandwidth Factor for White Noise, I_2	0.562
Noise Bandwidth Factor for f^2 noise, I_3	0.0868
Boltzmann Constant, k	$1.3806488 \times 10^{-23} \text{ J/K}$
Absolute Temperature, T_A	300 K

$$SNR = \frac{c_1(A_{pd})^2(P_t)^2}{c_2A_{pd}P_tB + c_3A_{pd}B + c_4A_{pd}B^2 + c_5(A_{pd})^2B^3} \quad (13)$$

where

$$\begin{aligned} c_1 &= \gamma^2 \left[\frac{(m+1)}{2\pi d^2} (\cos\varphi)^m T_s g(\psi) \cos(\psi) \right]^2, \\ c_2 &= 2q\gamma \left[\frac{(m+1)}{2\pi d^2} (\cos\varphi)^m T_s g(\psi) \cos(\psi) \right], \\ c_3 &= 2q\gamma I_2 E_{det} T_s n^2, \\ c_4 &= \frac{8\pi k T_A}{G} \eta I_2, \\ c_5 &= \frac{16\pi^2 k T_A \Gamma}{g_m} \eta^2 I_3. \end{aligned}$$

The values of c_1 , c_2 , c_3 , c_4 and c_5 can be determined based on the system parameters in Table I.

We reformulated the SNR in (13) in terms of two objective functions, namely $f_1(x)$ and $f_2(x)$, where $f_1(x)$ represents the received electrical signal component, and $f_2(x)$ denotes the total noise variance:

$$SNR = \frac{f_1(x)}{f_2(x)} = \frac{c_1 x_1^2 x_2^2}{c_2 x_1 x_2 x_3 + c_3 x_1 x_3 + c_4 x_1 x_3^2 + c_5 x_1^2 x_3^3} \quad (14)$$

where $x_1 = A_{pd}$, $x_2 = P_t$, and $x_3 = B$.

Our goal is to maximize $f_1(x)$ and minimize $f_2(x)$ concurrently, subject to the following constraints:

$$x_1 \leq 50 \times 10^{-4} \quad (1a)$$

$$x_2 \leq 2 \quad (1b)$$

$$x_3 > 0 \quad (1c)$$

All three variables, x_1 , x_2 , and x_3 are positive parameters because A_{pd} , P_t , and B cannot be negative.

Constraint 1a imposes a limit on the maximum photodetector area A_{pd} ; i.e., the detector area should not occupy more than 50 percent of the face of a CubeSat. This constraint ensures that there is enough space reserved for other surface-mounted optics and electronics, such as LED array. The unit of the photodetector active area is in m^2 , and we assume the standard specification of the face of a 1U Cubesat - which is $10 \text{ cm} \times 10 \text{ cm}$.

The second constraint, 1b, places a bound on the maximum transmitted optical power P_t . The transmitted optical power P_t is capped at $2W$ in order to ensure that it is consistent with the typical power requirement of the communication subsystem of a 1U CubeSat [20].

Constraint 1c represents the receiver bandwidth in Hz and it is assumed to be greater than zero. The noise variance increases with increase in the receiver bandwidth.

V. OPTIMAL PARAMETERS SELECTION AND ANALYSIS

In this section, we employed the NSGA II to determine the Pareto front of the two objective functions. This approach uses a controlled elitist genetic algorithm (GA), which favors individuals with a better fitness value [8]. The controlled elitist GA also favors individuals that can help increase the diversity of the population for convergence to the Pareto optimal front. In this instance, a population is a set of points in the design space. The initial population is generated randomly by default. The next generation of the population is computed using the non-dominated rank and a distance measure of the individuals in the current generation [21].

Using the design space (i.e., variable bounds) specified in Table II, we invoked MATLAB's gamultiobj solver which uses NSGA II to find the Pareto front of the two objective functions. The values of c_1 , c_2 , c_3 , c_4 and c_5 were determined based on the parameter values in Table I.

TABLE II: Objective Functions To Be Minimized

Variable Bounds	Objective (or Fitness) functions
$0.001 \leq x_1 \leq 0.005$	$f_1(x) = -c_1 x_1^2 x_2^2$
$0.5 \leq x_2 \leq 2$	$f_2(x) = c_2 x_1 x_2 x_3 + c_3 x_1 x_3 +$
$500000 \leq x_3 \leq 10000000$	$c_4 x_1 x_3^2 + c_5 x_1^2 x_3^3$

Table III and Fig. 2 display 25 solutions found on the Pareto front after 109 iterations, and depicts the trade-off between Objective 1 and 2 (i.e., $f_1(x)$ and $f_2(x)$), respectively. These solutions are non-dominated in the sense that one objective cannot be improved without sacrificing the other. However, they provide designers deeper insight into the quantitative trade-off among objectives and the many options available for implementation.

Although the Pareto solutions are equally good from the perspectives of the given objectives, it is the task of the communication system designer to select an optimal solution

TABLE III: Pareto Front and Corresponding Design Variables

$f_1(x)$	$f_2(x)$	(x_1, x_2, x_3)
12.2413×10^{-4}	5.41×10^{-5}	(0.003628, 1.9705, 531724)
0.9940×10^{-4}	1.81×10^{-5}	(0.001212, 1.6813, 531205)
13.1391×10^{-4}	5.51×10^{-5}	(0.003724, 1.9891, 527441)
4.0100×10^{-4}	3.04×10^{-5}	(0.002059, 1.9878, 525716)
22.4988×10^{-4}	7.23×10^{-5}	(0.004858, 1.9954, 530297)
17.2241×10^{-4}	6.27×10^{-5}	(0.004268, 1.9872, 523841)
3.0900×10^{-4}	2.86×10^{-5}	(0.001928, 1.8632, 528078)
23.6994×10^{-4}	7.86×10^{-5}	(0.004985, 1.9956, 562075)
23.6573×10^{-4}	7.59×10^{-5}	(0.004981, 1.9956, 543130)
18.0057×10^{-4}	6.41×10^{-5}	(0.004346, 1.9952, 525455)
9.7800×10^{-4}	4.79×10^{-5}	(0.003209, 1.9916, 531583)
7.4700×10^{-4}	4.16×10^{-5}	(0.002806, 1.9899, 529069)
7.3700×10^{-4}	4.11×10^{-5}	(0.002790, 1.9886, 525421)
8.8800×10^{-4}	4.51×10^{-5}	(0.003065, 1.9865, 524993)
6.3800×10^{-4}	4.01×10^{-5}	(0.002709, 1.9049, 527762)
19.4934×10^{-4}	6.65×10^{-5}	(0.004523, 1.9953, 524554)
11.2183×10^{-4}	5.10×10^{-5}	(0.003453, 1.9827, 527108)
13.9366×10^{-4}	5.67×10^{-5}	(0.003844, 1.9850, 525586)
21.6813×10^{-4}	7.09×10^{-5}	(0.004769, 1.9955, 529834)
11.7896×10^{-4}	5.26×10^{-5}	(0.003517, 1.9952, 533232)
14.8640×10^{-4}	5.94×10^{-5}	(0.003976, 1.9815, 532139)
16.4668×10^{-4}	6.14×10^{-5}	(0.004164, 1.9918, 526082)
2.4600×10^{-4}	2.54×10^{-5}	(0.001706, 1.8785, 531305)
2.0000×10^{-4}	2.25×10^{-5}	(0.001523, 1.8971, 527876)
6.81×10^{-6}	1.46×10^{-5}	(0.001004, 0.5315, 518040)

from the Pareto front. In this paper, we selected the optimal solution from the Pareto front using TOPSIS. According to this technique [7], the selected optimal solution should have the smallest Euclidean distance from the ideal solution and also the largest Euclidean distance from the negative-ideal solution. The ideal solution is a combination of the best value of each objective in the given optimal solutions. In contrast, the negative-ideal solution refers to the worst value of each objective in the given optimal solutions [7].

Following the approach in [7], the optimal solution within the design space in Table II was found to be as shown in Fig. 3. The algorithm selected the point $(0.0023657, 7.59 \times 10^{-5})$ as the optimal solution. This solution corresponds to the design variables $(x_1, x_2, x_3) = (0.004981, 1.9956, 543130)$ in

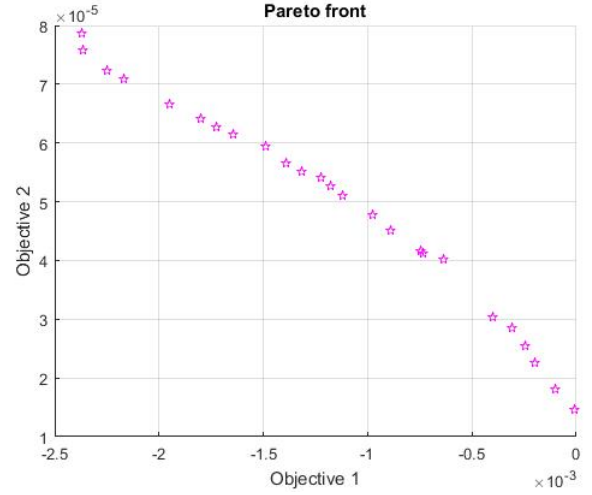


Fig. 2: Pareto Front of $f_1(x)$ and $f_2(x)$

Table III and produces a SNR of 15 dB. Analysis of all the parameter values in Table III clearly shows that the selected solution is optimal and has the maximum SNR within the set of possible solutions. In other words, using a combination of active detector area $A_{pd} = 0.004981 \text{ m}^2$, transmitted optical power of $P_t = 1.9956 \text{ W}$ and receiver bandwidth $B = 543130 \text{ Hz}$ or $(0.54313) \text{ MHz}$ will yield the maximum SNR from the possible set of solutions at the Pareto front.

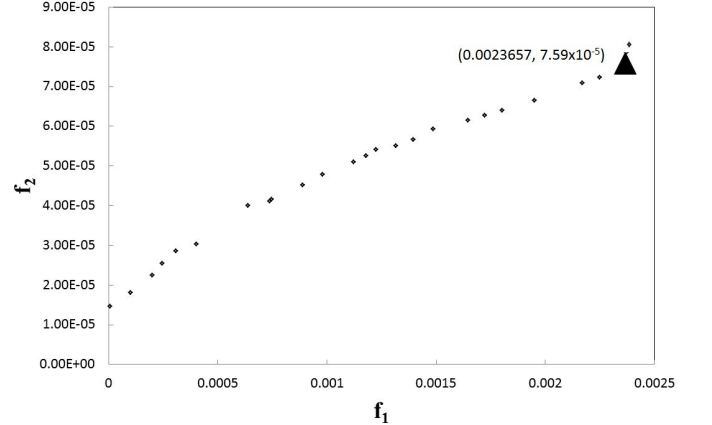


Fig. 3: TOPSIS Optimal Solution at Pareto Front

From the foregoing, it can be concluded that the optimal solution that maximizes the SNR in (14) over the design space in Table II is $(x_1, x_2, x_3) = (0.004981, 1.9956, 543130)$. This understanding of the impact of LED transmit power P_t , photodetector area A_{pd} , and bandwidth B on SNR will be useful in the decision making process of a link-budget. The careful selection of these parameters via optimization techniques can be used as a first step in improving the SNR at the receiver. Advanced digital modulation techniques can subsequently be employed to further improve the link performance or BER, which is a function of SNR.

VI. COMPARATIVE EVALUATION OF LINK PERFORMANCE WITH AND WITHOUT OPTIMIZATION

For the same design space in Table II, we compared the SNR (dB) of the inter-satellite link for the case where the design parameter values were selected without the aid of optimization techniques [5] and for the scenario where multi-objective optimization techniques were employed to determine optimal parameter values. The parameter values are as shown in Table IV.

TABLE IV: Example Parameter Values

Design Parameter	Value (Without Optimization)	Value (With Optimization)
A_{pd} (m^2)	0.000784	0.004981
P_t (W)	2	1.9956
B (Hz)	500000	543130

For a link distance of 1 km, Fig. 4 depict the SNR for the two different scenarios. It is significant to note an improvement of the SNR by an average value of about 7 dB as a result of the application of multi-objective optimization techniques to select design variable values. Even more significant, is the marginal increase (or improvement) of the SNR as the channel become noisier as illustrated in Fig. 4.

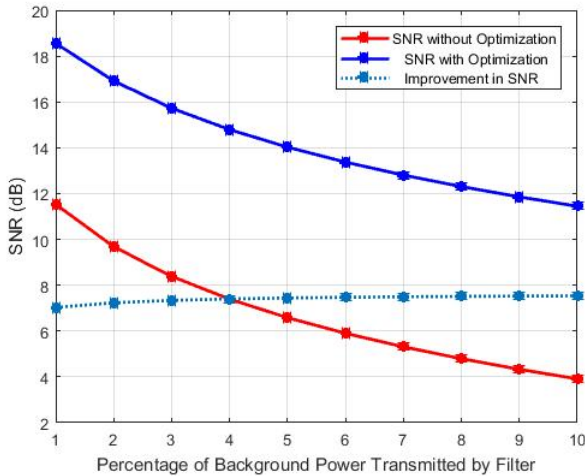


Fig. 4: Gain in SNR due to Optimization

VII. CONCLUSION

The size limitations of small satellites limit the extent to which we can increase physical layer design parameters such as the photodetector active area, LED transmit power, and receiver bandwidth. A sub-optimal allocation of these resources could lead to poor SNR at the receiver. However, a careful application of multi-objective optimization techniques can be used to achieve the required balance of these resources, and serve as a first step in obtaining the desired SNR at the receiver.

In this paper, we showed that the SNR of an LED-based VLC system for ISC can be improved by more than 3 dB through application of multi-objective optimization and selection methods during the decision making process of assigning design parameter values compared to the scenario where parameter values are chosen based on personal judgement.

REFERENCES

- [1] S. Rajagopal, R. Roberts, and S. Lim, "IEEE 802.15.7 Visible Light Communication: Modulation Schemes and Dimming Support," *IEEE Communication Magazine*, vol. 50, no. 3, pp. 72–82, Mar. 2012.
- [2] L. Wood, W. Ivancic, and K. Dorpelkus, "Using Light-Emitting Diodes for Intersatellite Links," in *2010 IEEE Aerospace Conference*, Big Sky, MT, 2010, pp. 1–6.
- [3] C. Poly, *CubeSat Design Specification*, rev. 12 ed., California Polytechnic State University, Cal Poly SLO, Aerospace Engineering Dept.
- [4] S. S. Board, "Achieving science with cubesats - thinking inside the box," National Academy of Sciences, Engineering and Medicine, Tech. Rep., 2016. [Online]. Available: <https://www.nap.edu/catalog/23503/achieving-science-with-cubesats-thinking-inside-the-box>
- [5] D. Amanor, W. Edmonson, and F. Afghah, "Utility of Light Emitting Diodes for Inter-Satellite Communication in Multi-Satellite Networks," in *2016 IEEE International Conference on Wireless for Space and Extreme Environments (WiSEE)*, Aachen, 2016, pp. 117–122.
- [6] T. Komine, "Fundamental Analysis for Visible-Light Communication System using LED Lights," *IEEE Transactions on Consumer Electronics*, vol. 50, pp. 100–107, 2004.
- [7] Z. Wang and G. Rangaiah, "Application and analysis of methods for selecting an optimal solution from the pareto-optimal front obtained by multi-objective optimization," *American Chemical Society*, vol. 56, pp. 560–574, 2016.
- [8] S. Sharma, G. Rangaiah, and K. Cheah, "Multi-objective optimization using ms excel with an application to design of a falling-film evaporator system," *The Institution of Chemical Engineers: Published by Elsevier B.V.*, vol. 90, pp. 123–134, 2011.
- [9] S. Hranilovic and F. Kschischang, "Optical Intensity-Modulated Direct detection Channels: Signal Space and Lattice Codes," *IEEE Transactions on Information Theory*, vol. 49, 2003.
- [10] S. Hranilovic, *Wireless Optical Communication Systems*. Springer Science, 2005.
- [11] K. Cui *et al.*, "Line-of-sight Visible Light Communication System Design and Demonstration," in *Communication Systems Networks and Digital Signal Processing*, 2010.
- [12] J. Barry and J. Khan, "Link Design for Non-Directed Wireless Infrared Communications," *Applied Optics*, vol. 34, pp. 3764–3776, 1995.
- [13] J. Barry, *Wireless Infrared Communications*. Kluwer, 1994.
- [14] I. Lee *et al.*, "Performance Enhancement of Outdoor Visible-Light Communication System using Selective Combining Receiver," *IET Optoelectronics*, vol. 3, pp. 30–39, 2009.
- [15] W. Spencer, "Fourier Series Representation of the Sun," *Search*, vol. 2, p. 172, 1971.
- [16] NASA-AMES, "Mars Climate Modeling Center," <http://spacescience.arc.nasa.gov/mars-climate-modeling-group/brief.html>, accessed online on 29 March 2016. [Online]. Available: <http://spacescience.arc.nasa.gov/mars-climate-modeling-group/brief.html>
- [17] NASA, "Brief description of 1-d radiation code in general circulation model," NASA AMES, Mars Climate Modeling Center, Tech. Rep., 2011.
- [18] S. Trisno, "Design and Analysis of Advanced Free Space Optical Communication Systems," Ph.D. dissertation, University of Maryland, 2006.
- [19] D. Amanor, W. Edmonson, and A. Anyanahun, "Visible light communication system for inter-satellite communication of small satellites," in *Small Satellites Systems and Services (4S) Symposium*, Valletta, Malta, 2016. [Online]. Available: <http://esaconferencebureau.com/4S2016/programme/proceedings>
- [20] R. Radakrishnan, W. W. Edmonson, F. Afghah, R. M. Rodriguez-Osorio, F. Pinto, and S. Burleigh, "Survey of Inter-satellite Communication for Small Satellites Systems: Physical layer to network layer view," *IEEE Communications Surveys and Tutorials*, vol. 18, no. 4, pp. 2442–2473, 2016, fourth Quarter.
- [21] K. Deb, A. Pratap, and T. Meyarivan, "A fast and elitist multiobjective genetic algorithm: Nsga ii," *IEEE Transactions on Evolutionary Computation*, vol. 6, no. 2, pp. 182–197, Apr. 2002.